Efficient radiative transfer techniques in hydrodynamic simulations

A. Mercer[1,⋆], D. Stamatellos[1] & A. Dunhill[1]
[1] *Jeremiah Horrocks Institute for Mathematics, Physics & Astronomy, University of Central Lancashire, Preston, PR1 2HE, UK*

Accepted XXX. Received YYY; in original form ZZZ

ABSTRACT
Radiative transfer is an important component of hydrodynamic simulations as it determines the thermal properties of a physical system. It is especially important in cases where heating and cooling regulate significant processes, such as in the collapse of molecular clouds, the development of gravitational instabilities in protostellar discs, disc-planet interactions, and planet migration. We compare two approximate radiative transfer methods which indirectly estimate optical depths within hydrodynamic simulations using two different metrics: (i) the gravitational potential and density of the gas (Stamatellos et al.), and (ii) the pressure scale-height (Lombardi et al.). We find that both methods are accurate for spherical configurations e.g. in collapsing molecular clouds and within clumps that form in protostellar discs. However, the pressure scale-height approach is more accurate in protostellar discs (low and high-mass discs, discs with spiral features, discs with embedded planets). We also investigate the β-cooling approximation which is commonly used when simulating protostellar discs, and in which the cooling time is proportional to the orbital period of the gas. We demonstrate that the use of a constant β cannot capture the wide range of spatial and temporal variations of cooling in protostellar discs, which may affect the development of gravitational instabilities, planet migration, planet mass growth, and the orbital properties of planets.

Key words: hydrodynamics - radiative transfer - methods: numerical - protoplanetary systems: planet-disc interactions, protoplanetary discs

1 INTRODUCTION

Full 3-dimensional, wavelength dependent radiative transfer within hydrodynamic simulations is computationally expensive (e.g. Harries 2015; Harries et al. 2017). It is only typically used to post-process snapshots of simulations to produce synthetic observations (e.g. RADMC-3D; Dullemond 2012). However, the inclusion of radiative transfer is important when an accurate treatment of the thermal evolution of the system is needed.

There are various methods which efficiently include approximate radiative transfer in hydrodynamic simulations, each with their underlying simplifying assumptions (Oxley & Woolfson 2003; Whitehouse & Bate 2004; Stamatellos et al. 2007b; Forgan et al. 2009; Young et al. 2012; Lombardi et al. 2015). There are two main types of approach: (i) using the diffusion approximation (e.g. Whitehouse & Bate 2004; Boley et al. 2006; Commerçon et al. 2011b,a), a method which may still be computationally expensive, or (ii) use a metric to estimate the optical depth for each element of the fluid and hence the heating/cooling rate (Stamatellos et al. 2007b; Forgan et al. 2009; Young et al. 2012; Lombardi et al. 2015). Another method that is used in the context of protostellar discs is the β-cooling approximation (e.g. Gammie 2001; Rice et al. 2003b). This method assumes that the temporal evolution of the specific internal energy, u, is inversely proportional to the cooling time such that $\dot{u} = -u/t_{\rm cool}$. The cooling time is set inversely proportional to the Keplerian frequency with a constant β, i.e. $t_{\rm cool}(R) = \beta\Omega^{-1}(R)$, where R is the distance from the central star as measured on the disc midplane. This method over-simplifies the underlying physics but comes at low computational cost.

Stamatellos et al. (2007b) proposed a radiative transfer method which uses the gravitational potential and the density of gas as a metric to estimate the optical depth through which a gas element cools. This is then used to calculate an estimated cooling rate, and, in the optically thick case, reduces to the diffusion approximation. The method works well for roughly spherical systems and results in an increase of computational time by less than $\sim 5\%$. However, Wilkins & Clarke (2012) showed that the cooling rate calculated with the Stamatellos et al. (2007b) method can be systematically underestimated in the optically thick midplane of protostellar discs. Therefore, the Stamatellos et al. (2007b) method therefore may not be suitable to provide accurate cooling rates in non-spherical systems. This method has been combined with the diffusion approximation to increase accuracy in high-optical depth regions (e.g. Forgan et al. 2009).

Young et al. (2012) proposed a method, in the context of protostellar discs, that uses the gravitational potential in the z direction only, i.e. out of the disc midplane. From this, they obtain accurate estimates (within a few tens of percent) of column density and optical depths. However, when fragments form due to the gravitational instability in massive discs, the Stamatellos et al. (2007b) gives better estimates of the cooling rates within the dense fragments, which can be assumed to be approximately spherical.

Instead of using the gravitational potential to estimate the opti-

⋆ E-mail: apmercer@uclan.ac.uk

cal depth, Lombardi et al. (2015) propose to use the pressure scale-height. This retains the majority of the characteristics of the original Stamatellos et al. (2007b) method, merely employing a different metric to estimate optical depth. It is shown to provide a much more accurate estimate of cooling rate in spherical polytropes and protostellar discs with specified density and temperature profiles.

The aim of this paper is to compare how the above methods (Stamatellos et al. 2007b; Lombardi et al. 2015), behave when applied in actual hydrodynamic simulations. We test the two methods in the context of collapsing clouds and protostellar discs. In the case of the latter, we consider relaxed discs, discs with spiral arms, discs with clumps, and discs with embedded planets which carve gaps. We also examine whether the β-cooling method, which is widely used for protostellar discs, provides a good approximation to the thermal physics. Such tests of different methods are needed as radiative transfer plays a critical role in many cases (e.g. disc fragmentation and gap opening in discs with planets).

In Section 2 we describe the radiative transfer techniques in more detail. Section 3 shows the comparison between the aforementioned methods for the collapse of spherically-symmetric cloud. We test the behaviour of both methods for protostellar discs in Section 4 and for discs with embedded planets in Section 5. A discussion on the performance of the β-cooling approximation is presented in Section 6. A comparison to demonstrate the effect on dynamical evolution from the two radiative transfer methods discussed, as well as the β-cooling approximation, is presented in Section 7. We summarise our results in Section 8.

2 EFFICIENT RADIATIVE TRANSFER METHODS

The radiative transfer technique ascribed to Stamatellos et al. (2007b) is used to determine the heating and cooling of the gas. The method incorporates the effects from the rotational and vibrational degrees of freedom of H_2, the dissociation of H_2, ice melting, dust sublimation, bound-free, free-free, and electron scattering interactions. The equation of state used and the effect of each assumed constituent are described in detail in §3 of Stamatellos et al. (2007b). The heating/cooling rate requires an estimate of the column density through which the heating/cooling happens as well as the local opacity. It is expressed as

$$\frac{\mathrm{d}u}{\mathrm{d}t} = \frac{4\sigma_{\mathrm{SB}}\left(T_{\mathrm{BGR}}^4 - T^4\right)}{\bar{\Sigma}^2\bar{\kappa}_{\mathrm{R}}\left(\rho,T\right) + \kappa_{\mathrm{P}}^{-1}\left(\rho,T\right)}, \tag{1}$$

where σ_{SB} is the Stefan-Boltzmann constant, T_{BGR} is the pseudo-background temperature below which the gas cannot cool radiatively, $\bar{\Sigma}$ is the mass-weighted mean column density, and $\bar{\kappa}_{\mathrm{R}}$ and κ_{P} are the Rosseland- and Planck-mean opacities, respectively. In the original Stamatellos et al. (2007b) method, the estimated mass-weighted column density is found via the local density ρ and gravitational potential ψ such that

$$\bar{\Sigma} = \zeta\left(\frac{-\psi\rho}{4\pi G}\right)^{1/2}, \tag{2}$$

where $\zeta = 0.372$ is a dimensionless coefficient with a weak dependence on polytropic index (set to $n = 1.5$). Particles are assumed to be surrounded by a pseudo-cloud represented by a polytrope. A particle heats or cools according to the characteristic optical depth of its pseudo-cloud (wherein the particle can be located at any position to account for non-spherical local geometry). The optical depth can be found via

$$\tau = \bar{\Sigma}\bar{\kappa}. \tag{3}$$

When considering the collapse of a 1 $\mathrm{M}_\odot$ spherical cloud of gas, the method has been shown to produce similar results to the simulations of Masunaga & Inutsuka (2000), which is a 1-D hydrodynamic simulation where the radiative transfer is treated accurately (Stamatellos et al. 2007b).

Lombardi et al. (2015) argue that the use of the gravitational potential as a metric overestimates column densities and optical depths in non-spherical configurations such as discs. Instead, they propose the use of pressure scale-height as a metric for calculating the optical depth. This is because the pressure gradient is typically oriented in the direction in which the optical depth increases most rapidly, i.e. approximately perpendicular to the disc midplane. The Lombardi et al. (2015) form for the estimated mass-weighted column density is

$$\bar{\Sigma} = \zeta'\frac{P}{|\boldsymbol{a}_h|}, \tag{4}$$

where $\zeta' = 1.014$ is a dimensionless coefficient. P is the pressure of the gas and $\boldsymbol{a}_h$ the hydrodynamical acceleration (i.e. the acceleration without any gravitational nor viscous contribution). This quantity can be expressed in terms of the pressure gradient such that

$$\boldsymbol{a}_h = \frac{-\nabla P}{\rho}. \tag{5}$$

For either method, the required quantities are readily available in any hydrodynamic method.

For a given particle density and temperature, a density-sorted look-up table can be used to find: specific internal energy; mean-molecular mass; mass-weighted optical depth; Rosseland- and Planck-mean optical depths; ratio of specific heat capacities; and the first adiabatic index. This removes the requirement of calculating computationally-expensive integrals on-the-fly (see §2.2 of Stamatellos et al. (2007b)).

We note that although the above methods have been devised for Smooth Particle Hydrodynamics (Gingold & Monaghan 1977; Lucy 1977), they can be applied to grid-based (e.g. Fryxell et al. 2000) and meshless techniques (Lanson & Vila 2008; Gaburov & Nitadori 2011; Hopkins 2015).

3 CLOUD COLLAPSE

We utilise the Graphical Astrophysics code for N-body Dynamics and Lagrangian Fluids (GANDALF, Hubber et al. 2018) to perform simulations of a collapsing molecular cloud, using the Stamatellos et al. (2007b) and Lombardi et al. (2015) methods of estimating optical depths. The cloud is initially static, has a mass of 1.5 $\mathrm{M}_\odot$ and is isothermal with a temperature 5 K. The cloud is represented by $N \approx 2\times10^6$ SPH particles distributed such that the density profile of the cloud is uniform across its radius $R_{\mathrm{cloud}} = 10^4$ AU.

Figure 1 shows the evolution of the central density and temperature for the two methods of estimating optical depths. Initially, the cloud collapses almost isothermally and the core temperature increases slowly with increasing density. The core temperature starts to increase rapidly as the cloud becomes optically thick ($\rho \sim 10^{-13}$ g cm^{-3}). At $\sim$ 100 K the rotational degrees of freedom of molecular hydrogen are excited and the temperature increases at a slower rate as the gravitational energy is diverted away from heating the cloud. The increasing temperature leads to increased thermal pressure that is able to slow down the collapse and the first

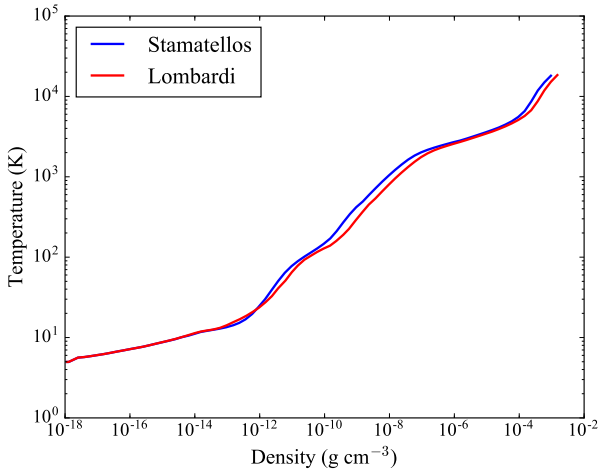

Figure 1. The evolution of central temperature as a function of central density for the collapse of an initially isothermal, non-rotating, 1.5 $M_\odot$ cloud with a radius of 10^4 AU. The radiative transfer methods of Stamatellos et al. (2007b) and Lombardi et al. (2015) are in good agreement.

hydrostatic core forms (Larson 1969; Masunaga & Inutsuka 2000; Whitehouse & Bate 2006; Stamatellos et al. 2007b). The first core contracts and heats slowly to $\sim$ 2000 K at which point hydrogen begins to dissociate. This results in the second collapse and the formation of the second hydrostatic core (the protostar).

The Lombardi et al. (2015) method gives similar results regarding the central density and temperature of the cloud with the Stamatellos et al. (2007b) method, which is turn compares very well with the Masunaga & Inutsuka (2000) method, indicating that both methods work reasonably well for spherical geometries. The second collapse in the case of the Stamatellos et al. (2007b) method is delayed by $\sim$ 100 yr, which may arise due to a slight overestimate in optical depth and thus less efficient cooling, as can be seen from the slightly higher temperatures calculated by this method (see Fig. 1).

4 PROTOSTELLAR DISCS

Protostellar discs form due to the turbulence and/or initial rotation of their progenitor molecular clouds. Their study is important as they are the birthplace of planets, which can form either through core accretion (e.g Safronov & Zvjagina 1969; Lissauer 1993), or by gravitational fragmentation of discs (Whitworth & Stamatellos 2006; Stamatellos et al. 2007a; Stamatellos & Whitworth 2009; Kratter et al. 2010; Zhu et al. 2012). Massive protostellar discs fragment if two conditions are met: (i) They are gravitationally unstable i.e.

$$Q \equiv \frac{\kappa c_s}{\pi G \Sigma} < Q_{\rm crit}, \tag{6}$$

where Q is the Toomre parameter (Toomre 1964), κ is the epicyclic frequency, c_s is the local sound speed and Σ is the disc surface density. The value of $Q_{\rm crit}$ is on the order of unity. (ii) They cool sufficiently fast, i.e. $t_{\rm COOL} < (0.5-2)t_{\rm ORB}$, where $t_{\rm ORB}$ is the local orbital period (Gammie 2001; Johnson & Gammie 2003; Rice et al. 2003b, 2005). Both requirements are dependent on the thermal properties of the disc, and so it is important that the cooling rate and the disc temperature are accurately calculated with the employed radiative transfer method.

Here, we present comparisons of estimated optical depth and cooling rate obtained via the Stamatellos et al. (2007b) and Lombardi et al. (2015) radiative transfer methods. In Section 4.1 we present our comparison methodology. Section 4.2 considers a low-mass relaxed disc. Section 4.3 considers a high-mass disc which fragments forming spiral arms (Section 4.4) and eventually gravitationally bound clumps (Section 4.5).

4.1 Methodology

We use the Graphical Astrophysics code for N-body Dynamics and Lagrangian Fluids (GANDALF, Hubber et al. 2018) to perform simulations protostellar discs (§4) and protostellar discs with embedded planets (§5). From these simulations we select snapshots for which we compare the behaviour of the Stamatellos et al. (2007b) and Lombardi et al. (2015) radiative transfer methods.

The estimated column density for both the gravitational potential and pressure scale-height metrics, $\bar{\Sigma} \equiv \Sigma_{\rm est}$, is found by post-processing a snapshot of the GANDALF hydrodynamic simulation. The corresponding estimated optical depth is $\bar{\tau} \equiv \tau_{\rm est} = \Sigma_{\rm est}\bar{\kappa}_{\rm R}$, where $\bar{\kappa}_{\rm R}$ is the mass-weighted opacity for each method (note that this is slightly different for the two methods, see Lombardi et al. (2015)). The column density and optical depth are calculated for each particle in the simulation. We emphasise that we calculate the optical depths and cooling rates for the same snapshots for both methods, i.e. using the same density and temperature disc configurations. We provide azimuthally-averaged radial profiles of the optical depth and cooling rates at the disc midplane (defined such as $|z| < 0.5$ AU) and also vertical to the disc midplane profiles of the same quantities. We also calculate the actual values of column density and optical depth by integrating from the gas element which we consider, to the disc surface along the z-axis (perpendicular to the disc midplane) such that $\Sigma_{\rm actual} = \int \rho \, {\rm d}z$ and $\tau_{\rm actual} = \int \kappa\left(\rho, T\right) \rho \, {\rm d}z$.

The estimated cooling-rate per unit mass can then be found via Equation 1. We normalise this with respect to $4\sigma_{\rm SB}\left(T^4 - T_{\rm BGR}^4\right)$ such that we define the quantity

$$\dot{u}_{\rm est} \equiv -\left.\frac{{\rm d}u}{{\rm d}t}\right|_{\rm est} \frac{1}{4\sigma_{\rm SB}\left(T^4 - T_{\rm BGR}^4\right)} = \frac{1}{\bar{\Sigma}^2\bar{\kappa}_{\rm R} + \kappa_{\rm P}^{-1}} \tag{7}$$

to represent the estimated cooling-rate per unit mass. We compare this with the actual cooling-rate per unit mass which is calculated using the actual optical depth and column density, hence

$$\dot{u}_{\rm actual} \equiv -\left.\frac{{\rm d}u}{{\rm d}t}\right|_{\rm actual} \frac{1}{4\sigma_{\rm SB}\left(T^4 - T_{\rm BGR}^4\right)} = \frac{1}{\Sigma\left(\tau_{\rm R} + \tau_{\rm P}^{-1}\right)}, \tag{8}$$

where $\tau_{\rm R}$ and $\tau_{\rm P}$ are the optical depths calculated using the Rosseland-mean and Planck-mean opacities, respectively (which in many cases are assumed to be the same). We note that the above equation is itself an approximation to the diffusion approximation (Mihalas 1970) in which the radiative flux is

$$F = -\frac{4}{3\kappa_{\rm R}\rho}\nabla\left(\sigma_{\rm SB}T^4\right). \tag{9}$$

From this, we obtain the cooling rate per unit mass which is

$$\dot{u} = \frac{1}{\rho}\nabla\cdot F \approx \frac{\sigma_{\rm SB}T^4}{\kappa_{\rm R}\Sigma^2} \approx \frac{\sigma_{\rm SB}T^4}{\tau_{\rm R}\Sigma}, \tag{10}$$

and has the same form of Equation 8 in the optically thick limit.

4.2 Relaxed low-mass disc

We simulate a protostellar disc with a mass of $0.01\,\mathrm{M}_\odot$ around a $1\,\mathrm{M}_\odot$ protostar. $N \approx 2\times10^6$ SPH particles are distributed between radii of 5 and 100 AU such that the initial column density and temperature profiles follow $\Sigma(R) \propto R^{-1}$ and $T(R) \propto R^{-1/2}$, respectively. The temperature at 1 AU from the central star is $T_0 = 250$ K. The disc is heated by an ambient radiation field of 10 K.

A steady-state is reached after a few outer orbital periods, shown in Figure 2a. The disc is optically thin, thus both the Stamatellos and Lombardi methods provide accurate cooling rate estimates (see Figure 2b). However, the Stamatellos method generally overestimates the optical depth, especially in the inner disc, consequently underestimating the cooling rate. We also take an annulus of the disc between 34 and 36 AU and show the azimuthally-averaged vertical profiles of optical depth and cooling rate (Figure 2d, e). The cooling rate from the disc midplane to the surface is accurately estimated as the region is optically thin. In this regime, the optical depth is not important for calculating the cooling rate (see Equation 1).

4.3 High-mass disc

We simulate a massive protostellar disc which develops spiral features, undergoes fragmentation, forming dense, gravitationally-bound clumps. The disc has an initial mass of $0.2\,\mathrm{M}_\odot$ and attends a $0.8\,\mathrm{M}_\odot$ protostar. $N \approx 2 \times 10^6$ SPH particles are distributed between radii of 5 and 100 AU such that the initial column density and temperature profiles follow $\Sigma(R) \propto R^{-1}$ and $T(R) \propto R^{-1/2}$, respectively. The temperature at 1 AU from the central star is $T_0 = 250$ K. The disc is heated by an ambient radiation field of 10 K.

Figure 3a shows the column density of the disc before any significant dynamical evolution occurs. The disc midplane is optically thick (out to a radius of $\sim$ 30 AU), but the optical depth does not drop below $\tau = 0.1$ further out (Figure 3b). The Stamatellos method overestimates the optical depth by a factor of a few throughout the disc. The Lombardi method yields a better estimate for both the optical depth and the cooling rate. Similar results are found when considering the vertical profiles of these quantities in a radial annulus between 34 and 36 AU (Figure 3d, e).

4.4 High-mass disc with spiral arms

After some time, the disc becomes unstable and spiral arms begin to form. This is shown in Figure 4a. The optical depth and cooling rate at the disc midplane are well described by the Lombardi method, but are over- and underestimated, respectively, by the Stamatellos method. The cooling rate estimated by the Stamatellos method is in agreement with the actual value when the disc is optically thin (Figure 4b). We consider two cylindrical regions with base radius of 5 AU wherein we perform vertical analyses: one cylinder is inside a spiral arm and and the other outside (see marked regions in Figure 4a). Outside the spiral arm, the disc is optically thin and the cooling rate is estimated well by both methods (Figure 4e, dashed lines). However, inside the spiral arm where the disc is optically thick, the Stamatellos method overestimates the optical depth and therefore the cooling rate. The Lombardi method provides more accurate values for both quantities (Figure 4e, solid lines).

4.5 High-mass disc with clumps

The disc eventually fragments and dense clumps form. The column density snapshot in Figure 5a contains four clumps. The central density of the densest clump is $\sim 10^{-6}$ g cm^{-3} and for the least dense clump is $\sim 10^{-10}$ g cm^{-3}. Figure 5b shows that both the Stamatellos and Lombardi methods give good estimates of the azimuthally-averaged optical depth at the disc midplane, but it should be noted that an azimuthally-averaged analysis is not ideal for describing this disc, as it is highly non-axisymmetric. Therefore we focus on two of the clumps: the inner, densest clump, and the least dense clump. We consider a cylinder with base radius of 5 AU centred on each of these clumps and we perform a vertical analysis in the direction perpendicular to the disc midplane. Figure 5d shows the optical depth comparison. We find that for the least dense clump (dashed lines), the Stamatellos method is accurate in the centre of the clump. The Lombardi method overestimates the optical depth by a factor $\sim$ 2. In the centre of the densest clump, both methods are inaccurate, but only by a factor of a few. In general - for the disc as a whole as well as the clumps - the Lombardi method estimates the cooling rate well, whilst the Stamatellos method systematically underestimates the cooling rate.

5 PROTOSTELLAR DISCS WITH EMBEDDED PLANETS

The gravitational interaction between a planet and the surrounding disc may result in the formation of planet-induced gaps (e.g. Goldreich & Tremaine 1980; Lin & Papaloizou 1993; Bryden et al. 1999; Kley & Nelson 2012). Such structures may provide indirect evidence for the presence of planets in discs. The Crida et al. (2006) semi-analytical criterion for gap formation involves the balance between the tidal torque which opens the gap and the viscous torque which closes the gap. It has been shown that planets with masses down to $10\,\mathrm{M}_\oplus$ can open gaps (Duffell & MacFadyen 2012). However, for migrating planets, a gap must form on a rapid enough timescale. Malik et al. (2015) argue that a gap can only form provided the gap opening time is longer than the migration timescale of the planet. The accurate treatment of the radiative transfer in such planet-disc systems is important and may play a significant role when determining the rate and the direction (i.e. inwards or outwards) of migration, and the final mass of the planet (Stamatellos 2015; Benítez-Llambay et al. 2015; Stamatellos & Inutsuka 2018).

Here we examine two cases of protostellar discs with embedded planets: one with an embedded $1.4\,\mathrm{M}_\mathrm{J}$ planet (§5.1) and one with an embedded higher-mass, $11\,\mathrm{M}_\mathrm{J}$, planet (§5.2). We compare the estimated optical depth and cooling rate obtained via the Stamatellos et al. (2007b) and Lombardi et al. (2015) radiative transfer methods.

5.1 Disc with an embedded $1.4\,\mathrm{M}_\mathrm{J}$ planet

We consider a disc with an initial mass $0.005\,\mathrm{M}_\odot$ surrounding a $1\,\mathrm{M}_\odot$ protostar. A $1\,\mathrm{M}_\mathrm{J}$ mass planet is embedded within the disc at a radius of 5.2 AU. The initial disc extends out to 15.6 AU, with a surface density profile $\Sigma(R) \propto R^{-1/2}$ (e.g. Bate et al. 2003), temperature profile $T(R) \propto R^{-3/4}$, and is represented by 10^6 SPH particles. The temperature at 1 AU from the central star is $T_0 = 250$ K. The planet migrates slightly inwards (0.1 AU) and increases in mass by accreting gas from the disc. At the snapshot presented

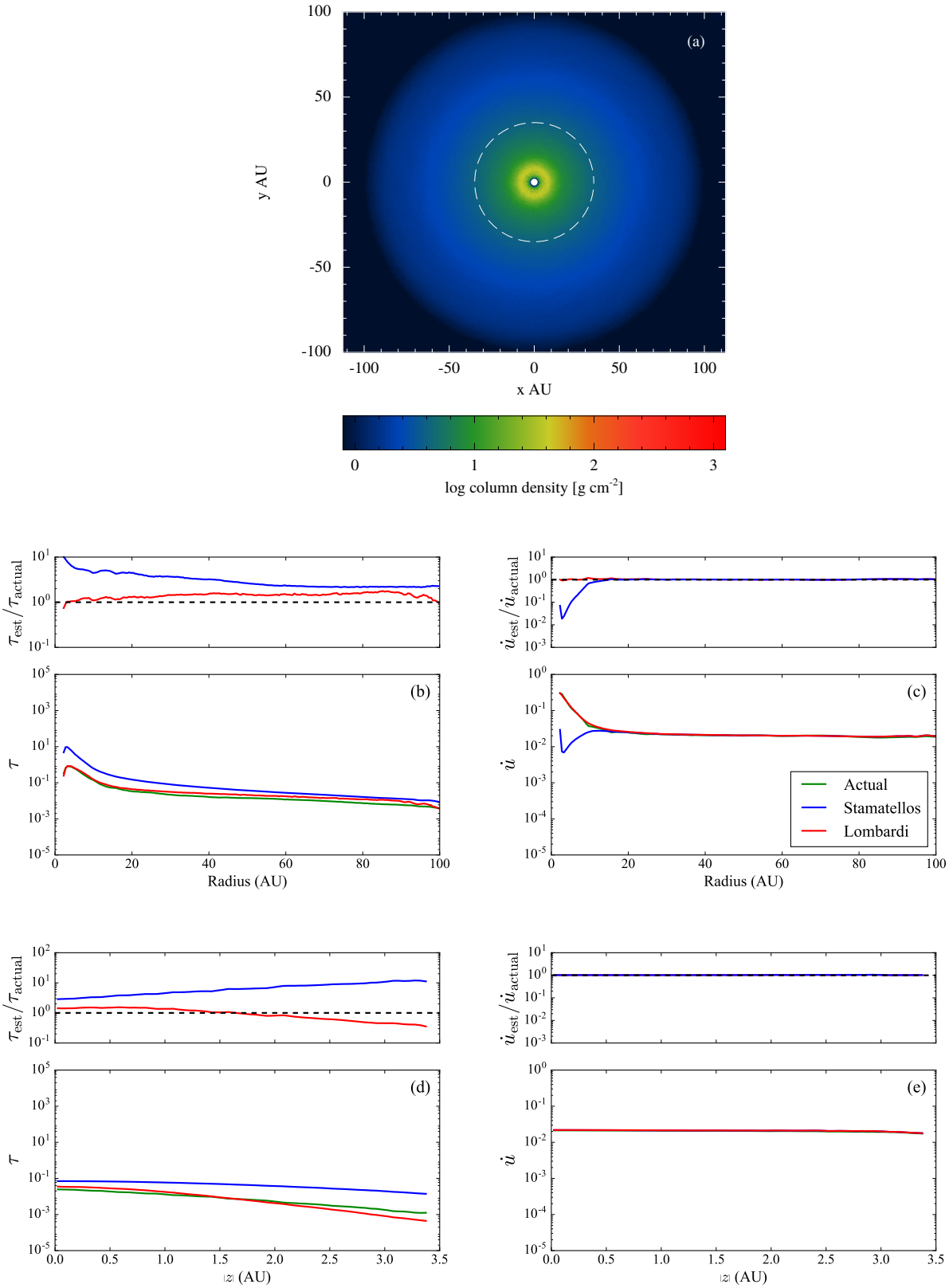

Figure 2. A low-mass disc which has evolved for a few outer orbital periods and has reached a steady-state. Panel (a): a column density snapshot where the dashed white line represents the radius at which we perform an analysis perpendicular to the disc midplane. Panels (b) and (c): comparisons of azimuthally-averaged optical depth and cooling rate at the disc midplane ($|z| < 0.5$ AU). Panels (d) and (e): azimuthally-averaged optical depth and cooling rate perpendicular to the disc midplane for a radial annulus of $34 - 36$ AU. The upper plots in panels (b-e) show the ratio between estimated and actual values. The black dashed lines represent equality. The disc is optically thin, and as such, both methods give good estimates of the cooling rate. The Stamatellos method generally overestimates the optical depth at the disc midplane, especially in the inner disc region, consequently underestimating the cooling rate.

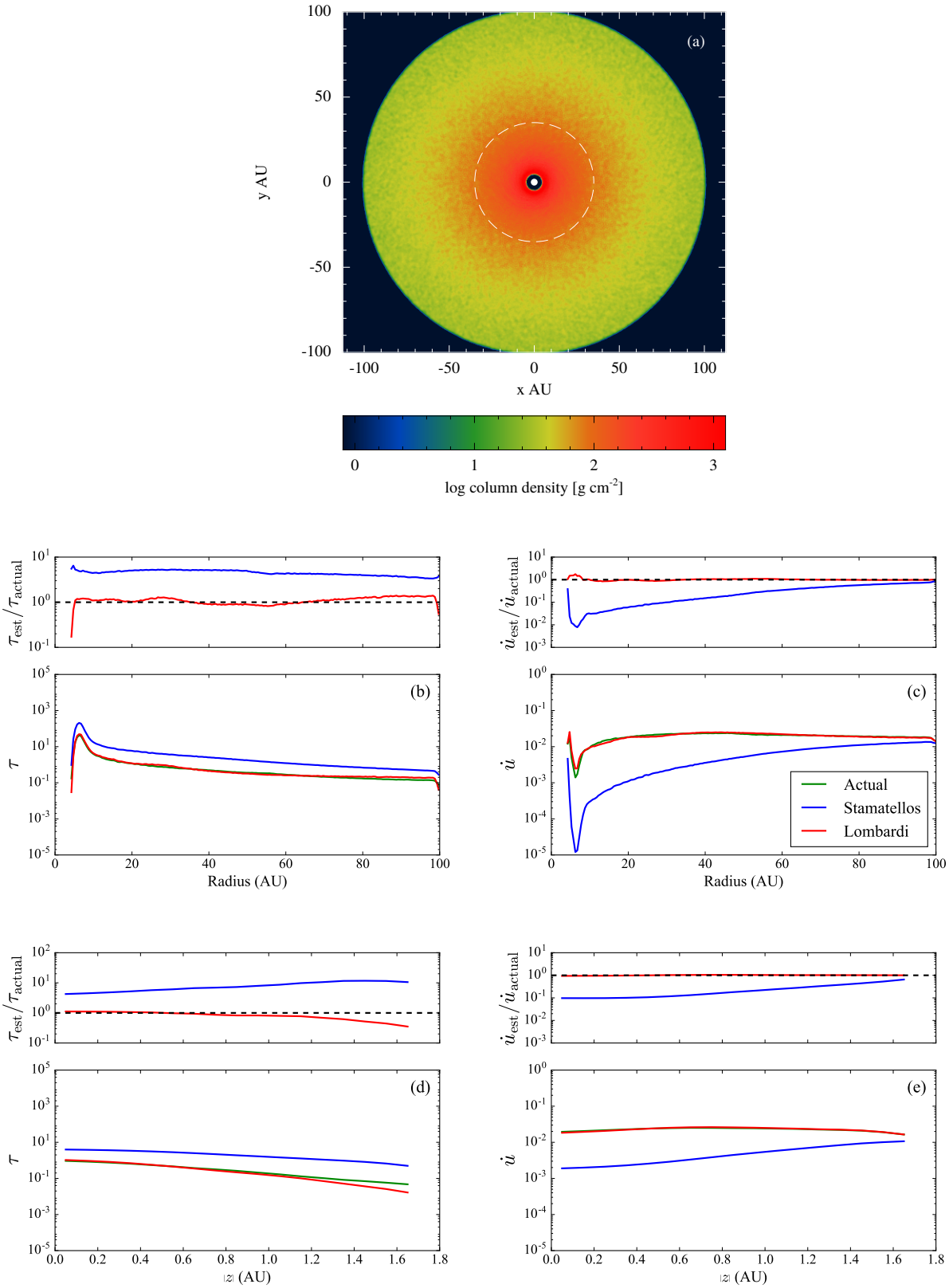

Figure 3. A high-mass disc which has not yet undergone significant evolution. Panel (a): a column density snapshot where the dashed white line represents the radius at which we perform an analysis perpendicular to the disc midplane. Panels (b) and (c): comparisons of azimuthally-averaged optical depth and cooling rate at the disc midplane. Panels (d) and (e): azimuthally-averaged optical depth and cooling rate perpendicular to the disc midplane for a radial annulus of $34 - 36$ AU. The upper plots in panels (b-e) show the ratio between estimated and actual values. The black dashed lines represent equality. The Stamatellos method overestimates the optical depth at the disc midplane by a factor ~ 5 at all disc radii, but the Lombardi method yields a more accurate estimate. This is reflected in the cooling rate. Similar results are found when considering the optical depth and cooling profiles perpendicular to the disc midplane (d-e).

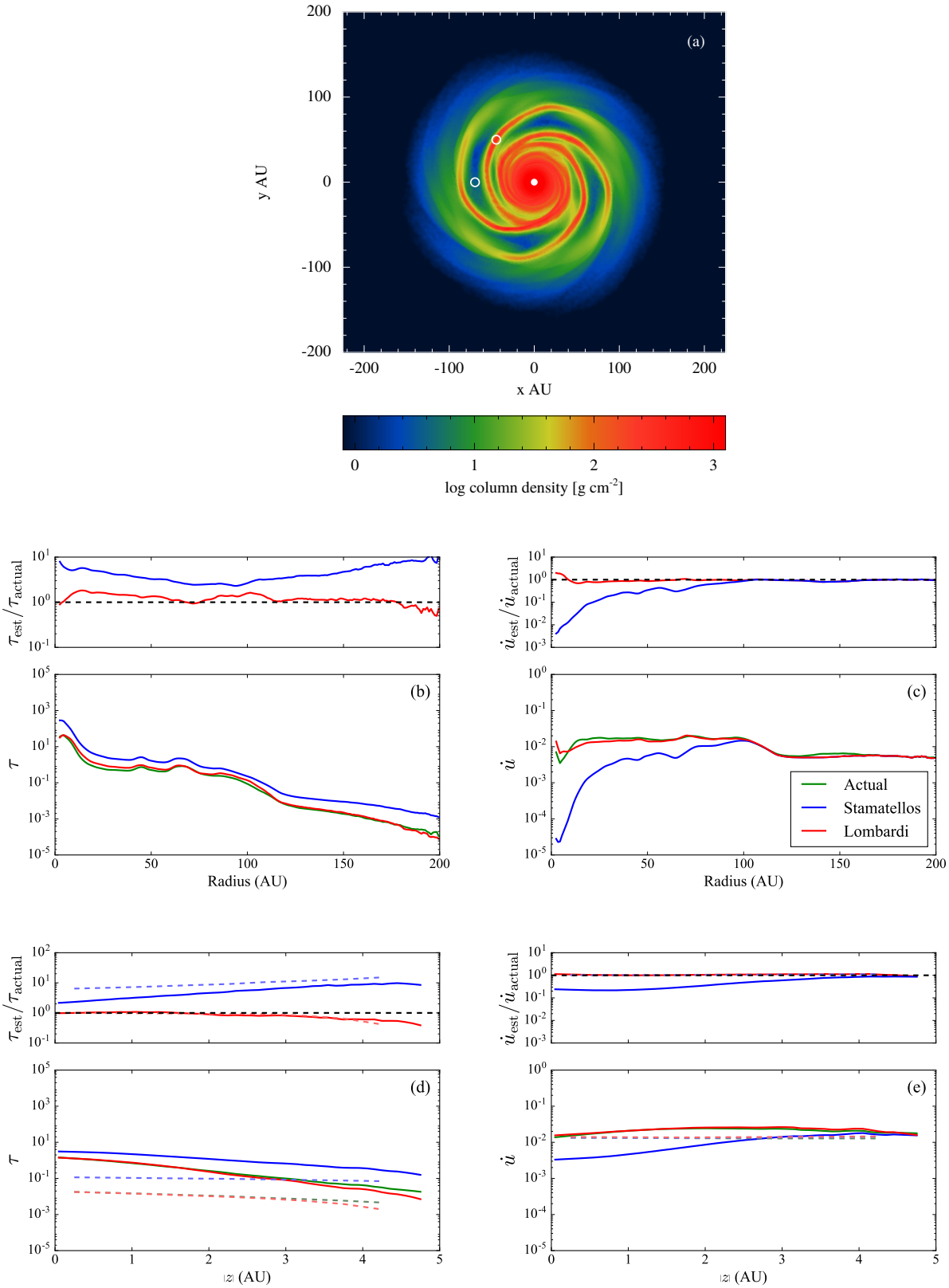

Figure 4. A high-mass disc which has evolved to form spiral arms. Panel (a): a column density snapshot. White circles represent cylindrical regions where we perform an analysis perpendicular to the disc midplane. Panels (b) and (c): comparisons of azimuthally-averaged optical depth and cooling rate at the disc midplane. Panels (d) and (e): optical depth and cooling rate comparisons perpendicular to the disc midplane inside (solid lines), and outside (dashed lines) of a spiral arm. The upper plots in panels (b-e) show the ratio between estimated and actual values. The black dashed lines represent equality. The optical depth and cooling rate at the disc midplane are well estimated by the Lombardi method at all disc radii, but are over- and underestimated by the Stamatellos method, respectively. Vertically to the disc midplane, the same result is observed within a spiral arm. However, outside of the spiral arms, where the disc is optically thin, both methods yield a good estimate for the cooling rate.

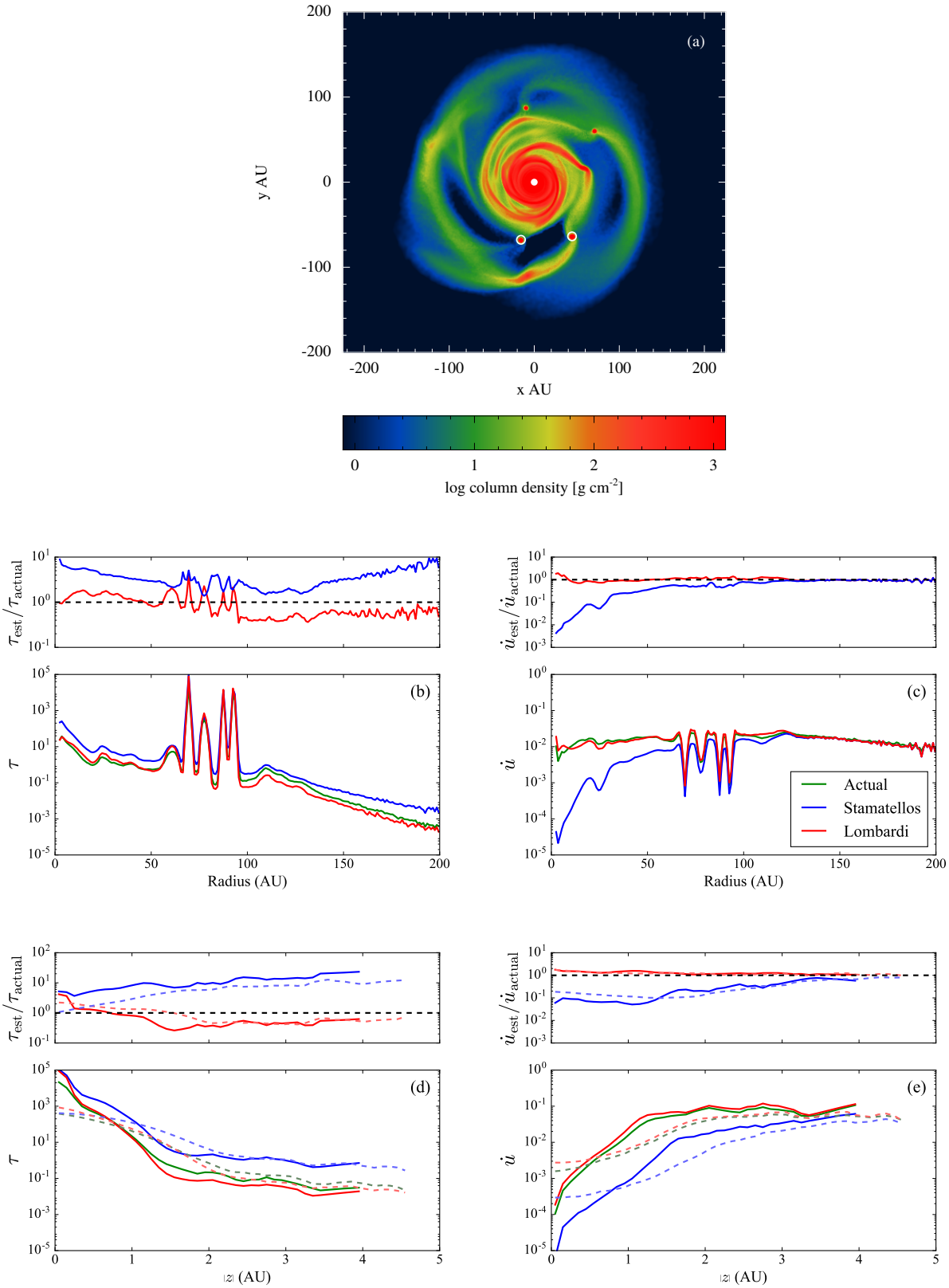

Figure 5. A high-mass disc which has evolved to form dense clumps. Panel (a): a column density snapshot. White circles represent regions where vertical analyses are performed. Panels (b) and (c): comparisons of azimuthally-averaged optical depth and cooling rate at the disc midplane. Panels (d) and (e): optical depth and cooling rate comparisons perpendicular to the disc midplane for the densest clump (solid lines), and the least dense clump (dashed lines). The upper plots in panels (b-e) show the ratio between estimated and actual values. The black dashed lines represent equality. The optical depth is generally overestimated by the Stamatellos method. The Lombardi method gives a better estimate, even within the dense clump. The cooling rate is also estimated more accurately.

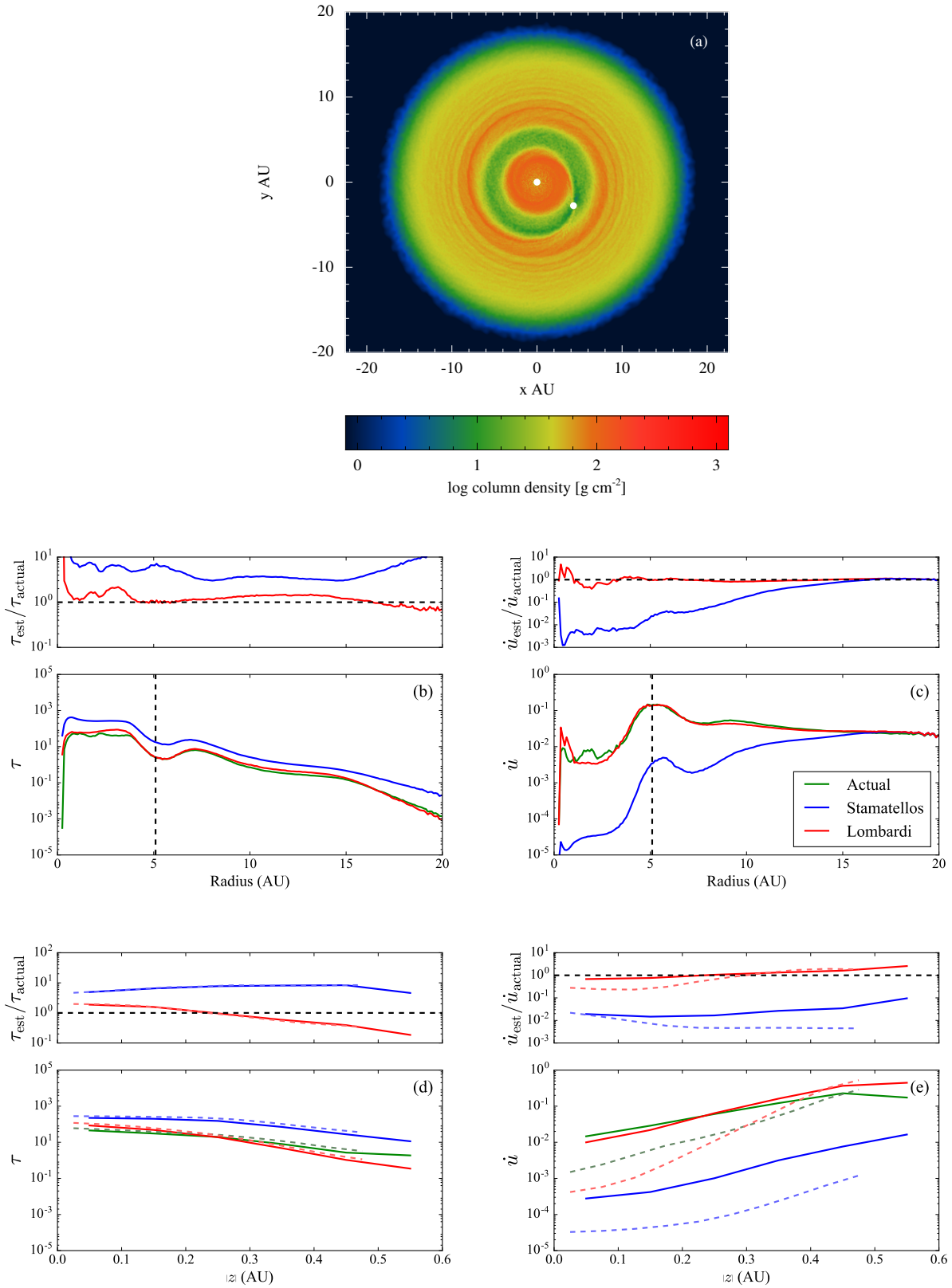

Figure 6. A disc which has an embedded $1.4\,{\rm M_J}$ planet at a radius of 5.1 AU. Panel (a): a column density snapshot. Panels (b) and (c): comparisons of azimuthally-averaged optical depth and cooling rate at the disc midplane. The vertical black dashed lines in panels (b) and (c) represent the location of the planet. Panels (d) and (e): optical depth and cooling rate comparisons perpendicular to the disc midplane between radial annuli of $4-6$ AU (in the gap, solid lines), and $3-4$ AU (interior to the gap, dashed lines). Gas within $R_{\rm HILL}=0.6$ AU of the planet is excluded when analysing the gap. The upper plots in panels (b-e) show the ratio between estimated and actual values. The black dashed lines represent equality. The Stamatellos method overestimates the optical depth by a factor of 3 or more throughout the disc. The Lombardi method estimates the optical depth within a factor of 2, and it also gives an accurate estimate of the cooling rate, both inside and outside the planet-induced gap.

here (Figure 6a) the planet is at 5.1 AU and has carved out a gap between 4 and 6 AU. Its mass has increased to 1.4 M_J.

The density of the disc is high and as such, the disc is optically thick (Figure 6b). The Stamatellos method overestimates the optical depth at the disc midplane throughout the disc by a factor of a few, whilst the Lombardi method provides a better estimate (accurate within a factor of ~ 2). This is reflected in the estimated cooling rates (Figure 6c).

Vertical profiles are shown for radial annuli at the planet gap ($4-6$ AU; Figure 6d, e - solid lines) as well as on a region interior to the gap ($3-4$ AU, Figure 6d, e - dashed lines). We exclude gas within the Hill radius ($R_{\rm HILL} = 0.6$ AU) of the planet when analysing the gap region. Both of these regions are optically thick. Again, the Lombardi method provides a better estimate for the optical depth and cooling rate.

In the gap region, which is important for the evolution of the planet, the Lombardi method is very accurate, whereas the Stamatellos method overestimates the optical depth, and therefore underestimates the cooling rate.

5.2 Disc with an embedded 11 M_J planet

We simulate a system comprising a star which has an initial mass 1 $M_\odot$, that is attended by a protostellar disc with mass 0.1 $M_\odot$ and initial radius 100 AU. The disc is modelled by 10^6 SPH particles, and has initial surface density and temperature profiles $\Sigma(R) \propto R^{-1}$ and $T(R) \propto R^{-3/4}$, respectively (Stamatellos 2015). The temperature at 1 AU from the central star is $T_0 = 250$ K. A planet with an initial mass 1 M_J is embedded in the disc at radius of 50 AU. At the snapshot we present (Figure 7a) the disc mass has dropped to 0.08 $M_\odot$ and the planet mass has increased to 11 M_J. The planet has migrated inwards and is located at a radial distance of 36 AU. It has carved a gap between ~ 30 and ~ 40 AU.

Figure 7b shows that the Lombardi method estimates the optical depth at the midplane of the disc well within the gap, but overestimates it by a factor of a few outside of the gap. The Stamatellos method overestimates the optical depth at all radii: by a factor of ~ 2 outside of the gap and ~ 10 within the gap.

We consider two radial annuli where we perform vertical analyses. One includes the gap (between 33 and 37 AU, Figure 7d, e - solid lines), the other a region interior to the gap (between 23 and 27 AU, Figure 7d, e - dashed lines). The disc is optically thin within the gap. Thus the cooling rate is well estimated by both methods. We exclude gas within the Hill radius of the planet ($R_{\rm HILL} = 8.0$ AU) when analysing the gap. The region interior to the gap is optically thick. The cooling rate is well estimated at all z by the Lombardi method, but the Stamatellos method underestimates the cooling rate by up to a factor of 10.

6 TESTING THE β-COOLING APPROXIMATION

The β-cooling approximation (e.g. Gammie 2001; Rice et al. 2003b) is a computationally inexpensive technique used when simulating accretion discs. This method assumes that the cooling rate at a given radius R within the disc, is inversely proportional to cooling time such that

$$\dot{u} = \frac{u}{t_{\rm cool}}, \tag{11}$$

where the cooling time is

$$t_{\rm cool} = \beta \Omega^{-1}. \tag{12}$$

Ω is the Keplerian frequency and β is a dimensionless parameter which is typically assumed to be between 1 and 20. Provided a disc is close to Toomre instability (i.e. $Q \approx 1$), a disc may only be able to fragment if the cooling is sufficiently fast (β on the order of a few). The critical value at which gravitational fragmentation occurs, $\beta_{\rm crit}$, is still debated. Meru & Bate (2011) suggest that the limit may be as high as $\beta_{\rm crit} \approx 30$. More recent studies by Baehr et al. (2017) suggest a value of $\beta_{\rm crit} = 3$.

In this section, we compare the β-cooling approximation with the cooling rates which we obtain from Equation 8 (which is what we refer to as *actual* cooling). We calculate an effective beta, $\beta_{\rm eff}$, in order to determine whether the assumption of a constant β is a reasonable approximation. Therefore, we define $\beta_{\rm eff}$ as

$$\beta_{\rm eff} = \frac{u}{\dot{u}}\Omega. \tag{13}$$

where

$$\dot{u} = \frac{4\sigma_{\rm SB}T^4}{\Sigma\left(\tau_{\rm R} + \tau_{\rm P}^{-1}\right)}. \tag{14}$$

We emphasise that when calculating u we use the detailed equation of state used by Stamatellos et al. (2007b) (see summary in Section 2).

We present the $\beta_{\rm eff}$ that we calculate for the snapshots of protostellar discs presented in Sections 4 and 5. Figure 8 shows the azimuthally-averaged $\beta_{\rm eff}$ at the disc midplane; Figure 9 shows the value of $\beta_{\rm eff}$ vertically towards the surface of the disc at the given regions; Figure 10 shows colour maps of $\beta_{\rm eff}$ at the disc midplane. We can see that $\beta_{\rm eff}$ varies significantly throughout different regions of each disc, between ~ 0.1 and ~ 200.

For the smooth axis-symmetric disc cases that we examine here (Figures 10a, b), $\beta_{\rm eff}$ is high in the inner disc regions ($\beta_{\rm eff} > 20$) but drops down to ~ 3 in the outer regions. For the disc with the spiral arms (Figure 10c), the spirals are regions where $\beta_{\rm eff} \sim 1$, hence cooling is efficient. Thus, spiral arms may be prone to gravitational collapse as thermal energy generated by the contraction of a forming gas clump can efficiently escape. The dense, bound clumps in Figure 10d cool inefficiently ($\beta_{\rm eff} \sim 200$), due to being extremely optically thick.

Figure 10e shows $\beta_{\rm eff}$ for a disc with a 1.4 M_J embedded planet. $\beta_{\rm eff}$ is high in the outer regions but is low within the planet gap. This may be attributed to the associated high and low optical depths, respectively, of these regions. For a disc with an embedded higher-mass 11 M_J planet (Figure 10f), the planet induces a high-density spiral wake which cools fast ($\beta_{\rm eff} \sim 1$), whereas the gap region cools slowly ($\beta_{\rm eff} > 50$). The region around the planet has a low $\beta_{\rm eff}$ (< 1) and thus cools more efficiently.

We see that, as expected, that a region of the disc cools inefficiently (slowly) when it is optically thin (low-density regions of the disc, e.g in gaps), efficiently (quickly) when it is just optically thick ($\tau \sim 1$, e.g. in spirals induced by gravitational instabilities or planets), and again inefficiently (slowly) when it becomes extremely optically thick (in clumps/fragments).

We conclude that the actual cooling rate in a protostellar disc varies radially, vertically and with time as the disc evolves. Significant variations are observed within dense clumps which form through gravitational fragmentation. This makes the β-cooling method a rather crude approximation of the disc thermal physics when considering highly dynamical systems.

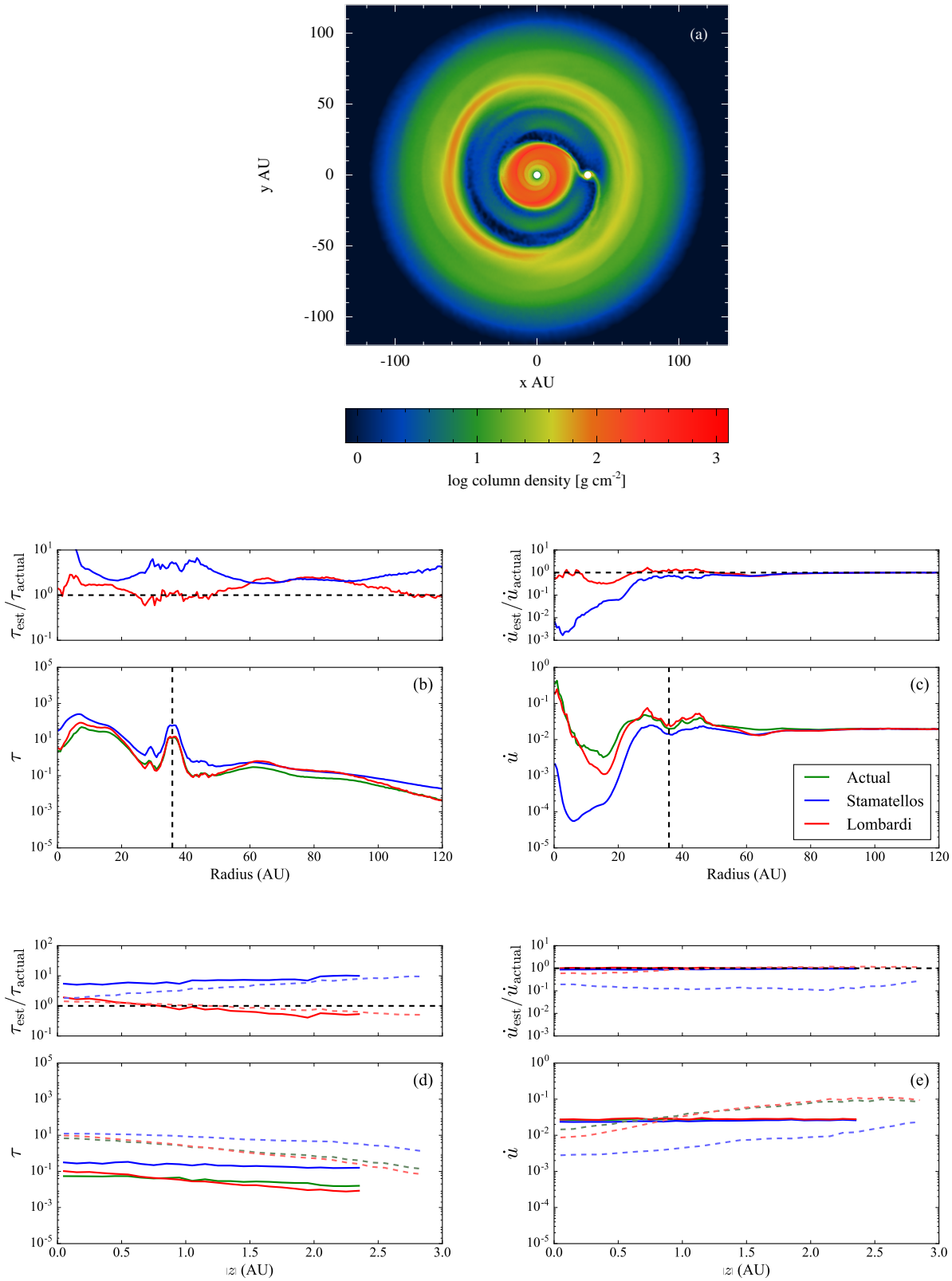

Figure 7. A disc which has an embedded 11 M_J planet at a radius of 36 AU. Panel (a): a column density snapshot. Panels (b) and (c): comparisons of azimuthally-averaged optical depth and cooling rate at the disc midplane. The vertical black dashed lines in panels (b) and (c) represent the location of the planet. Panels (d) and (e): optical depth and cooling rate comparisons perpendicular to the disc midplane between radial annuli of $33 - 37$ AU (inside the gap, solid lines), and $23 - 27$ AU (outside the gap, dashed lines). Gas within $R_{\rm HILL} = 8.0$ AU of the planet is excluded when analysing the gap. The upper plots in panels (b-e) show the ratio between estimated and actual values. The black dashed lines represent equality. Both methods overestimate the optical depth in the outer disc by a factor of 2 or 3. However, the Lombardi method estimates both the optical depth and the cooling within the gap more accurately than the Stamatellos method. Outside and within the gap, the Lombardi method gives a good estimate for both quantities from the disc midplane to the disc surface. The Stamatellos method estimates the cooling rate well within the gap as this region is optically thin.

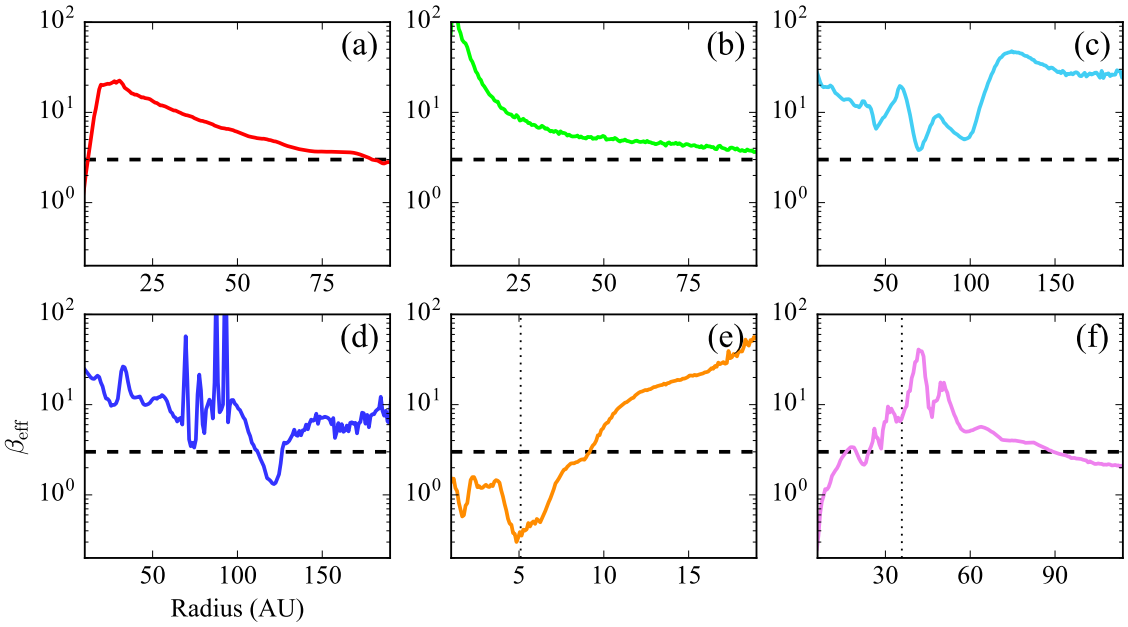

Figure 8. Azimuthally-averaged effective β at the disc midplane for the following snapshots: (a) a low-mass relaxed disc; (b) a high-mass disc; (c) a high-mass disc with spirals arms; (d) a high-mass disc with dense clumps; (e) a disc with an embedded 1.4 M_J planet; (f) a disc with an embedded higher-mass 11 M_J planet. Horizontal dashed lines represent $\beta_{\rm eff} = 3$. Vertical dotted lines represent the radii of planets (in the last two cases).

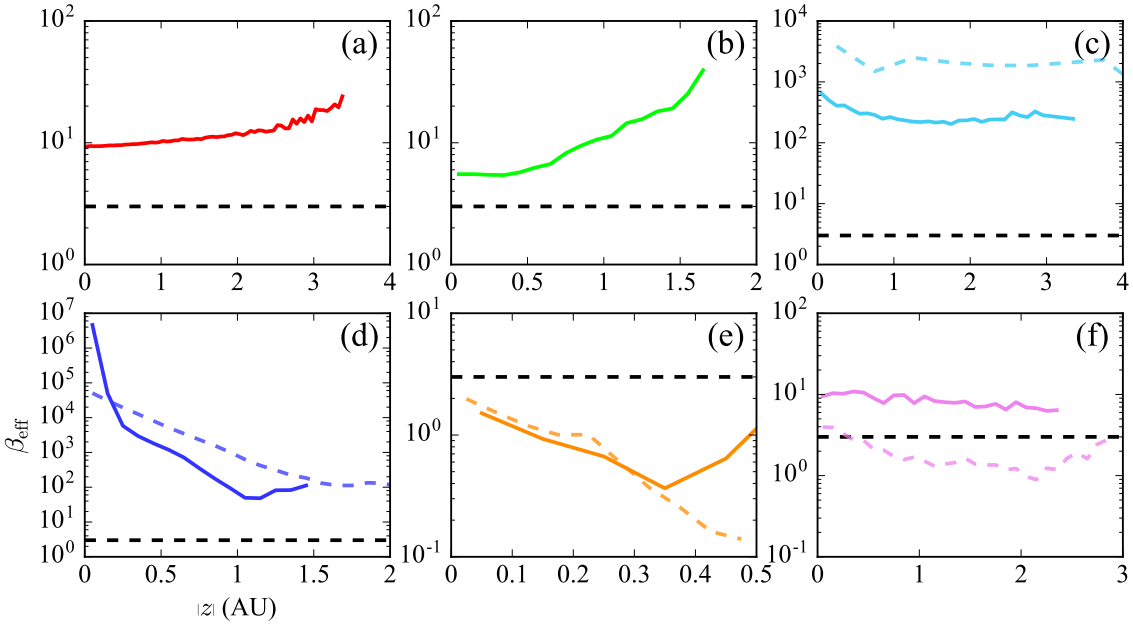

Figure 9. Effective β from the disc midplane to the disc surface for the following snapshots: (a) a low-mass relaxed disc (radial annulus $34 < R < 36$ AU); (b) a high-mass relaxed disc (radial annulus $34 < R < 36$ AU); (c) a disc with spirals arms (vertical cylinders with a base with radius of 5 AU regions centred within a spiral arm, solid line, and outside spiral arms, dashed line); (d) a disc with dense clumps (vertical cylinders with a base with radius of 5 AU centred within the densest clump, solid line, and the least dense clump, dashed line); (e) a disc with an embedded 1.4 M_J planet (radial annuli $4 < R < 6$ AU, solid line) and $3 < R < 4$ AU ,dashed line); (f) a disc with an embedded higher-mass 11 M_J planet (radial annuli $33 < R < 37$ AU, solid line) and $23 < R < 27$ AU, dashed line). Horizontal dashed lines represent $\beta_{\rm eff} = 3$.

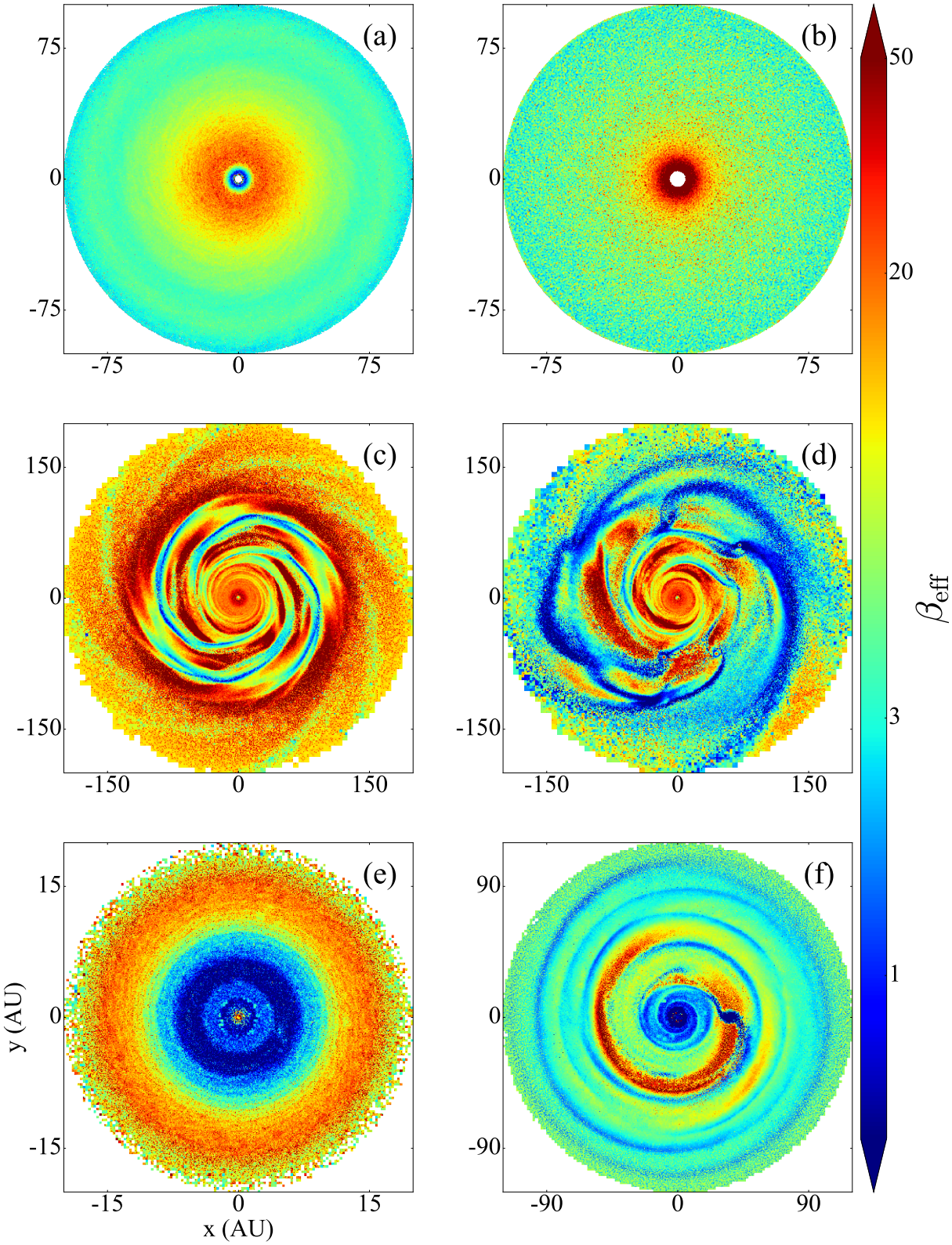

Figure 10. Effective β values at the disc midplane for the following snapshots: (a) a low-mass relaxed disc; (b) a high-mass disc; (c) a disc with spirals arms; (d) a disc with dense clumps; (e) a disc with an embedded 1.4 M_J planet; (f) a disc with an embedded higher-mass 11 M_J planet. Regions where $\beta_{\rm eff}$ is lower cool more efficiently. Gravitational instability is typically considered to occur for $\beta < 3$ provided that the Toomre parameter is also on the order of unity. We show that β varies across the disc, especially within spiral features and dense clumps. As such, it may not be appropriate to assume that β is constant throughout the disc.

7 DYNAMICAL EVOLUTION COMPARISON

We perform three simulations to demonstrate the differences that the β-cooling approximation, the Stamatellos et al. (2007b), and the Lombardi et al. (2015) radiative transfer methods exhibit. We simulate a $0.8\,\mathrm{M}_{\odot}$ protostar which is attended by a $0.2\,\mathrm{M}_{\odot}$ disc with surface density and temperature profiles $\Sigma(R) \propto R^{-1}$ and $T(R) \propto R^{-1/2}$, respectively. $N \approx 2 \times 10^{6}$ particles represent the disc, which is heated by a 10 K external radiative field. No heating from the central star is included. We test the β-cooling approximation with a value of $\beta = 3$, a limit at which cooling is efficient enough for gravitational instability to occur (Rice et al. 2003a).

Figure 11 shows the three discs after 1.5 kyr of evolution using: (a) the β-cooling approximation; (b) the Stamatellos radiative transfer method; and (c), the Lombardi radiative transfer method. We note that whilst all three discs become gravitationally unstable, the β-cooling approximation yields a more stable disc than the two radiative transfer methods. Due to a generally higher estimation of the cooling rate, the Lombardi method allows the disc to cool more efficiently and develop stronger spiral arms.

8 DISCUSSION

We have compared two approximate (but computationally inexpensive) methods to include radiative transfer in hydrodynamic simulations. These methods use two different metrics to calculate the optical depth through which the gas heats and cools: (i) the Stamatellos et al. (2007b) method uses the gravitational potential and the density, and (ii) the Lombardi et al. (2015) method instead uses the pressure scale-height.

We find that although both methods yield accurate estimates in the case of collapsing clouds, the use of the pressure scale-height metric to estimate optical depths (Lombardi et al. 2015) is more accurate when considering protostellar discs. We summarise our results in Figure 12, which illustrates the difference of optical depth estimation for the cases we examined in this paper for both methods. Using the pressure scale-height as a metric, a more accurate estimate of optical depth (by a factor of 2 or better) and cooling rate is obtained for protostellar discs in a variety of configurations: low-mass and high-mass discs, with or without an embedded planet, as well as gravitationally unstable discs which develop spiral arms and form bound clumps. The Stamatellos et al. (2007b) method may overestimate the optical depth by a factor of 10 in some cases, but the Lombardi et al. (2015) method is generally accurate within a factor of 3. Consequently, the Stamatellos et al. (2007b) method underestimates the cooling rate in optically thick protostellar discs, whereas the Lombardi et al. (2015) method provides better accuracy (although generally it also underestimates the cooling rate). Both methods give accurate estimates in the optically thin regime.

We also compare the cooling rates in hydrodynamic simulations of discs with those of the commonly used β-cooling approximation (e.g. Gammie 2001; Rice et al. 2003b). We find that using a constant value of β for a disc may not be a suitable approximation as this parameter may vary radially and vertically throughout the disc (between $\sim$ 0.1 and $\sim$ 200 in the cases that we examined here). It also varies with time as the disc evolves (e.g. when spiral arms and/or gaps form in the disc), but most significantly within dense clumps. The approximate radiative transfer methods discussed previously may be more appropriate to use as, at comparable computational cost, they are adaptive to the changes that happen as the disc evolves (e.g. the formation of spiral arms and clumps). Nevertheless, the β-cooling approximation is a useful parameterisation that facilitates greater control in numerical experiments considering the thermal behaviour of a disc.

Many hydrodynamic simulations of protostellar discs (in the context of e.g. disc evolution, disc fragmentation, disc-planet interactions, planet migration) have used such approximations for the radiative transfer to avoid excessive computational cost (e.g Rice et al. 2003a; Lodato & Rice 2004; Clarke et al. 2007; Lodato et al. 2007; Forgan & Rice 2009; Meru & Bate 2010; Stamatellos & Whitworth 2011; Ilee et al. 2017). Their results need to be seen in the context of the accuracy of the radiative transfer method used.

Studies of disc fragmentation (e.g Stamatellos & Whitworth 2009; Stamatellos et al. 2011) that use the Stamatellos et al. (2007b) method may have underestimated disc cooling by a factor of a few, so that their discs are less prone to fragmentation. This would mean that even discs with lower masses than the ones studied by Stamatellos et al. (2011) may be able to fragment (i.e. a disc with mass less than $0.25\,\mathrm{M}_{\odot}$ around a $0.7\,\mathrm{M}_{\odot}$ star). However, we should note that the uncertainties in the disc opacities could also be up to an order of magnitude, i.e. the uncertainty introduced is similar to that of the Stamatellos et al. (2007b) method.

Disc simulations using the β-cooling approximation also suffer from uncertainties in calculating cooling rates. For discs that start off optically thin, the cooling is inefficient (i.e. β_{eff} is large). The β_{eff} decreases (i.e. the cooling becomes more efficient) as the density increases in spiral arms and in the region around a planet (i.e. its circumplanetary disc). If the density continues to increase (i.e. if clumps form) the cooling becomes inefficient due to the high optical depth, and the β_{eff} increases. The use of a constant β misses this variation of cooling efficiency (both in space and time). Therefore the physics of disc fragmentation may not be captured appropriately. We demonstrate that a disc evolved using the β-cooling approximation, with a value of $\beta = 3$, results in a more stable disc as compared to similar simulations which employ the Stamatellos et al. (2007b) and Lombardi et al. (2015) radiative transfer methods (see Section 7).

In the case of planets embedded in discs, it has been suggested that efficient cooling promotes gas accretion (Nayakshin 2017; Stamatellos & Inutsuka 2018) and dust accretion (Humphries & Nayakshin 2018) onto the planet. Therefore, cooling rates may affect the mass growth of planets, their metallicity, and their associated circumplanetary discs. This in turn results in different migration rates, final masses and orbital characteristics for these planets e.g. as seen in Stamatellos (2015) in comparison with Baruteau et al. (2011) (see Stamatellos & Inutsuka 2018).

9 CONCLUSION

Approximate radiative transfer methods are useful due to their computational efficiency, but they should be treated with caution as radiative transfer may, in many cases, fundamentally affect the evolution of an astrophysical system. The Lombardi et al. (2015) method (that uses the pressure scale-height to calculate optical depths) is more accurate than the Stamatellos et al. (2007b) method (that uses the gravitational potential and the gas density as a proxy for optical depths) for disc simulations. Both methods behave accurately for spherical geometries (i.e. collapsing clouds or clumps in discs). When used for modelling protostellar discs, both methods are more accurate than the β-cooling approximation (at similar computa-

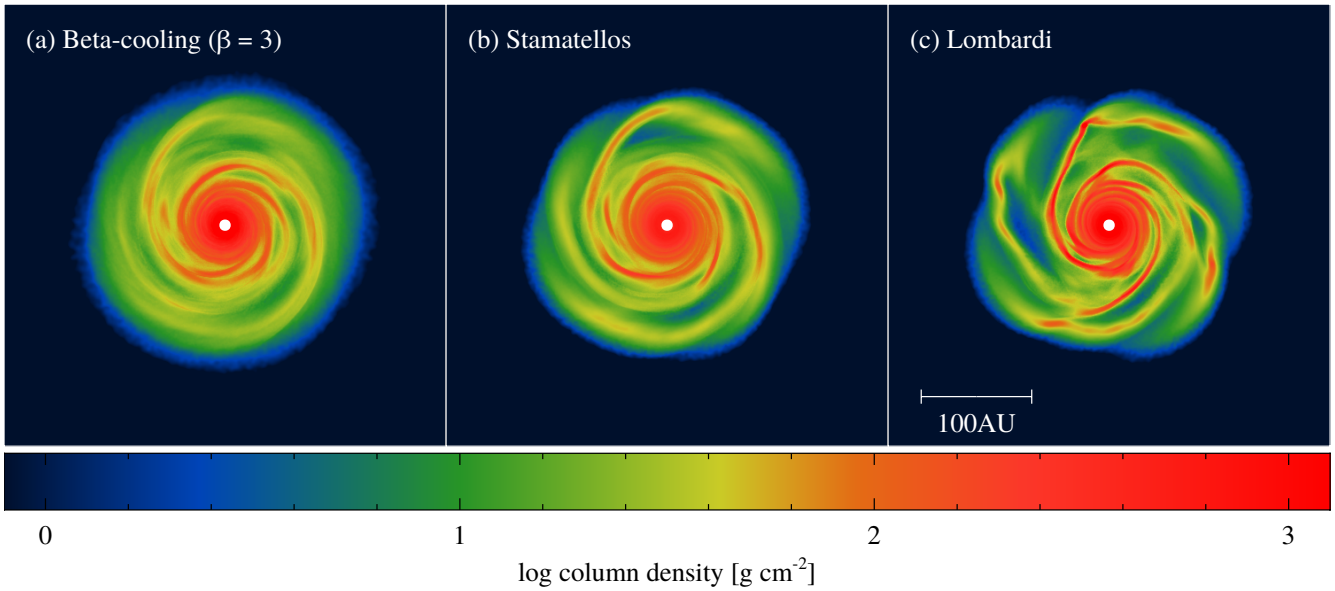

Figure 11. Surface density plots of a $0.2\,M_\odot$ disc around a $0.8\,M_\odot$ protostar after 1.5 kyr of evolution. Panel (a): a disc evolved using the β-cooling approximation with $\beta = 3$. Panel (b): a disc evolved using the Stamatellos et al. (2007b) radiative transfer method. Panel (c): a disc evolved using the Lombardi et al. (2015) method. Each disc becomes gravitationally unstable, but it is clear that the Lombardi disc (panel c) is more unstable, demonstrated by the stronger, more detailed spiral arms.

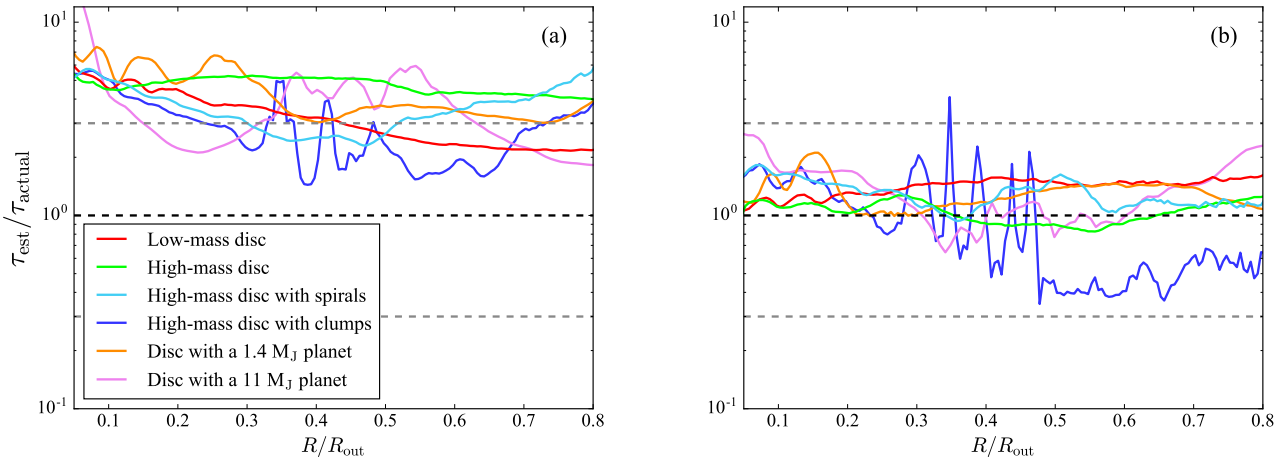

Figure 12. The ratio between estimated and actual optical depth for: (a) the Stamatellos et al. (2007b) method; (b) the Lombardi et al. (2015) method. Various disc configurations are shown. Radii have been normalised to the outer radius of each disc. The black dashed lines represent equal values of estimated and actual optical depth. The upper and lower grey dashed lines represent factors of 3 over- and underestimation respectively. The Lombardi et al. (2015) metric of estimating optical depths provides better accuracy in all cases presented. The optical depth is accurate by a factor of less than 3. The Stamatellos et al. (2007b) method is accurate within dense clumps/fragments.

tional cost), which nevertheless is a good tool for controlled numerical experiments of disc thermodynamics.

ACKNOWLEDGEMENTS

The authors would like to thank Richard Booth and David Hubber for the correspondence on the implementation of the methods used within this paper as well as useful comments. Thanks are given to the anonymous referee for constructive suggestions. Surface density plots were produced using the SPLASH software package (Price 2007). AM is supported by STFC grant ST/N504014/1. DS is partly supported by STFC grant ST/M000877/1. This work used the DiRAC Complexity system, operated by the University of Leicester IT Services, which forms part of the STFC DiRAC HPC Facility[1]. This equipment is funded by BIS National E-

[1] http://www.dirac.ac.uk

Infrastructure capital grant ST/K000373/1 and STFC DiRAC Operations grant ST/K0003259/1. DiRAC is part of the UK National E-Infrastructure.

REFERENCES

Baehr H., Klahr H., Kratter K. M., 2017, ApJ, 848, 40
Baruteau C., Meru F., Paardekooper S.-J., 2011, MNRAS, 416, 1971
Bate M. R., Lubow S. H., Ogilvie G. I., Miller K. A., 2003, MNRAS, 341, 213
Benítez-Llambay P., Masset F., Koenigsberger G., Szulágyi J., 2015, Nature, 520, 63
Boley A. C., Mejía A. C., Durisen R. H., Cai K., Pickett M. K., D'Alessio P., 2006, ApJ, 651, 517
Bryden G., Chen X., Lin D. N. C., Nelson R. P., Papaloizou J. C. B., 1999, ApJ, 514, 344
Clarke C. J., Harper-Clark E., Lodato G., 2007, MNRAS, 381, 1543
Commerçon B., Hennebelle P., Henning T., 2011a, ApJ, 742, L9
Commerçon B., Teyssier R., Audit E., Hennebelle P., Chabrier G., 2011b, eprint arXiv, 1102, 1216
Crida A., Morbidelli A., Masset F., 2006, Icarus, 181, 587
Duffell P. C., MacFadyen A. I., 2012, ApJ, 755, 7
Dullemond C. P., 2012, RADMC-3D: A multi-purpose radiative transfer tool, Astrophysics Source Code Library (ascl:1202.015)
Forgan D., Rice K., 2009, MNRAS, 400, 2022
Forgan D., Rice K., Stamatellos D., Whitworth A. P., 2009, MNRAS, 394, 882
Fryxell B., et al., 2000, ApJS, 131, 273
Gaburov E., Nitadori K., 2011, MNRAS, 414, 129
Gammie C. F., 2001, ApJ, 553, 174
Gingold R. A., Monaghan J. J., 1977, MNRAS, 181, 375
Goldreich P., Tremaine S., 1980, ApJ, 241, 425
Harries T. J., 2015, MNRAS, 448, 3156
Harries T. J., Douglas T. A., Ali A., 2017, MNRAS, 471, 4111
Hopkins P. F., 2015, MNRAS, 450, 53
Hubber D. A., Rosotti G. P., Booth R. A., 2018, MNRAS, 473, 1603
Humphries R. J., Nayakshin S., 2018, MNRAS, 477, 593
Ilee J. D., et al., 2017, MNRAS, 472, 189
Johnson B. M., Gammie C. F., 2003, ApJ, 597, 131
Kley W., Nelson R. P., 2012, ARA&A, 50, 211
Kratter K. M., Matzner C. D., Krumholz M. R., Klein R. I., 2010, ApJ, 708, 1585
Lanson N., Vila J.-P., 2008, SIAM J. Numer. Anal., 46, 1912
Larson R. B., 1969, MNRAS, 145, 271
Lin D. N. C., Papaloizou J. C. B., 1993, in Levy E. H., Lunine J. I., eds, Protostars and Planets III. pp 749–835
Lissauer J. J., 1993, ARA&A, 31, 129
Lodato G., Rice W. K. M., 2004, MNRAS, 351, 630
Lodato G., Meru F., Clarke C. J., Rice W. K. M., 2007, MNRAS, 374, 590
Lombardi J. C., McInally W. G., Faber J. A., 2015, MNRAS, 447, 25
Lucy L. B., 1977, AJ, 82, 1013
Malik M., Meru F., Mayer L., Meyer M., 2015, ApJ, 802, 56
Masunaga H., Inutsuka S., 2000, ApJ, 531, 350
Meru F., Bate M. R., 2010, MNRAS, p. 1504
Meru F., Bate M. R., 2011, MNRAS: Letters, 411, L1
Mihalas D., 1970, Stellar atmospheres. Series of Books in Astronomy and Astrophysics, San Francisco: Freeman
Nayakshin S., 2017, MNRAS, 470, 2387
Oxley S., Woolfson M. M., 2003, MNRAS, 343, 900
Price D. J., 2007, Publications of the Astronomical Society of Australia, 24, 159
Rice W. K. M., Armitage P. J., Bate M. R., Bonnell I. A., 2003a, MNRAS, 339, 1025
Rice W. K. M., Armitage P. J., Bonnell I. A., Bate M. R., Jeffers S. V., Vine S. G., 2003b, MNRAS, 346, L36
Rice W. K. M., Lodato G., Armitage P. J., 2005, MNRAS: Letters, 364, L56
Safronov V. S., Zvjagina E. V., 1969, Icarus, 10, 109
Stamatellos D., 2015, ApJ, 810, L11
Stamatellos D., Inutsuka S.-i., 2018, MNRAS,
Stamatellos D., Whitworth A. P., 2009, MNRAS, 392, 413
Stamatellos D., Whitworth A., 2011, Computational Star Formation, 270, 223
Stamatellos D., Hubber D. A., Whitworth A. P., 2007a, MNRAS: Letters, 382, L30
Stamatellos D., Whitworth A. P., Bisbas T., Goodwin S., 2007b, A&A, 475, 37
Stamatellos D., Maury A., Whitworth A., André P., 2011, MNRAS, 413, 1787
Toomre A., 1964, ApJ, 139, 1217
Whitehouse S. C., Bate M. R., 2004, MNRAS, 353, 1078
Whitehouse S. C., Bate M. R., 2006, MNRAS, 367, 32
Whitworth A. P., Stamatellos D., 2006, A&A, 458, 817
Wilkins D. R., Clarke C. J., 2012, MNRAS, 419, 3368
Young M. D., Bertram E., Moeckel N., Clarke C. J., 2012, MNRAS, 426, 1061
Zhu Z., Hartmann L., Nelson R. P., Gammie C. F., 2012, ApJ, 746, 110